A semi-implicit non-hydrostatic dynamical kernel using spectral representation in the horizontal and finite elements in the vertical.

Juan Simarro, Mariano Hortal

Agencia Estatal de Meteorología, Spain

2012, QJRMS

Abstract

The purpose of this work is to develop and test a vertical slice non hydrostatic model kernel as a first step to implement it in a full diabatic three dimensional numerical weather prediction model. The vertical coordinate has been chosen to be hybrid based on height. The spatial discretization is spectral in the horizontal dimension and cubic finite elements are used for the vertical discretization. The selected time stepping is a standard three time level semi-implicit scheme to avoid instabilities due to the presence of fast acoustic and gravity waves. The model has the option to run with Eulerian or semi-Lagrangian advection. A stability analysis of the linear model has been done. To evaluate the model stability and accuracy a set of test cases from the literature are presented in then linear and non linear regimes, with and without orography. We emphasize on the coordinate-independent formulation of each element of the model.

keywords: numerical weather prediction, dynamical kernel, non-hydrostatic, vertical finite elements.

1 Introduction

Non hydrostatic dynamics has been introduced in numerical weather prediction operations in many weather forecast centres. The quality of non hydrostatic dynamical kernels has been tested for a wide range of numerical techniques. The models that can be found are different in almost all the important numerical aspects, as the type of spatial discretization, the time stepping, the ability to preserve the total value of physical magnitudes, or the treatment of

the advection terms. Therefore, it is difficult to resume the existing non hydrostatic models.

In this paper we present a non hydrostatic dynamical kernel similar in various aspects to the ALADIN kernel (Bubnová et al., 1995; Bénard et al., 2010). The spectral technique is used for the horizontal spatial discretization and the time stepping is solved with a semi-implicit scheme. This combination allows, when the linearisation is performed around a horizontally homogeneous and constant in time reference atmosphere in hydrostatic equilibrium, the reduction of the full set of equations to a single three dimensional Helmholtz equation which can be solved exactly. The main differences between the scheme proposed here and the ALADIN kernel are the set of prognostic variables and the vertical spatial discretization. The vertical coordinate used in ALADIN is a mass based coordinate whereas the prognostic variables are carefully chosen to achieve stability (Bénard, 2003; Bénard et al. 2004; Bénard et al 2005).

The vertical coordinate used here is based on height. This vertical coordinate has disadvantages compared with the mass based coordinate as it is deduced from a linear stability analysis of the one dimensional vertical acoustic system in mass and height based coordinates (Bénard, 2003). However, it is shown (Bénard et al, 2004) that for height based vertical coordinate the full three dimensional set of Euler equations has an instability which is generally small. Both analysis show that height based coordinate is worse than the mass based coordinate from the point of view of the linear stability analysis of the Euler equations in an isothermal unbounded atmosphere. The reason to use a height based coordinate in this work is that, although potentially more unstable than the mass based coordinate, we have seen that after the spatial vertical discretization the range of stability is acceptable, and that height based coordinate has advantages in other aspects, which are fully exploited in this work. In fact, a number of non hydrostatic models operationally used for numerical weather prediction have height based vertical coordinate, although none of them have a horizontaly spectral discretization. For instance, the UM (Cullen, 1993), COSMO model (Doms and Schättler, 1997), MM5 model (Dudhia, 1993) and GEM model (Tanguay et al., 1990). An important advantage of the height based coordinate compared with the mass based coordi-

nate is that it is time independent and therefore the metric terms are constant in time. Moreover, the covariant formulation, also called coordinate-independent formulation, is applied straightforwardly to the Euler equations for time independent coordinates, but it is much more complicated in the case of time dependent coordinates (Luo and Bewkey, 2004). A second advantage of the height based coordinate is that the only vertical operators needed are the first and second derivative with respect to the vertical coordinate and it is not necessary to use integral operators as in the mass based coordinate case. The discrete versions of the differential and integral operators in the ALADIN model must verify a set of constraints to achieve stability (Bubnová et al., 1995) and the finite differences scheme used in the formulation of the vertical operators is chosen to fulfil the constraints. In turn, these constraints makes the implementation of high order accuracy vertical discretization difficult, as it is not easy to find both high order accurate integral and differential operators which satisfies this set of constraints. This problem does not appear in the height based coordinate case, and high order discretization can be used. In this work cubic vertical finite elements are applied for the discretization of the vertical derivative operators in a similar way to the ECMWF hydrostatic model (Untch and Hortal, 2004). Finally, a third advantage of using a height based vertical coordinate together with a covariant formulation is that lower and upper boundary conditions for the velocity are included in the semi-implicit solver and the velocity found after each time step verifies the boundary conditions. There is no need to use explicit values of the velocity in the implementation of the boundary conditions as in the ALADIN model (Bènard et al., 2010). These reasons have motivated to explore the possibility of using height based vertical coordinate in the context of a semi-implicit horizontally spectral model. To this end a two dimensional version of the dynamical kernel has been coded as a first step to implement it in a full three dimensional numerical weather prediction model.

In Section 2 the set of equations and boundary conditions in coordinate-independent form is presented. In section 3 the standard semi-implicit time stepping used is explained. The spatial discretization is exposed in section 4 except the discretization of the vertical operators, which are presented in section 5. A covariant version of the semi-Lagrangian advection

scheme is presented in section 6. The stability of the model is analysed in section 7. The results for a set of test cases taken from the literature are summarized in 8. Finally, conclusions are drawn in section 9.

2 Set of equations

For a dry atmosphere the chosen prognostic variables are the two dimensional velocity $\mathbf{v}(t,x,z)$ with components $u(t,x,z)$ and $w(t,x,z)$, the logarithm of temperature $r(t,x,z)$ and the logarithm of pressure $q(t,x,z)$. The set of Euler Equations in Cartesian coordinates for this prognostic variables is (Laprise, 1992)

$$\frac{d\mathbf{v}}{dt} + Re^r \nabla q + \nabla\phi = \mathbf{F} \tag{1}$$

$$\frac{dr}{dt} + \frac{R}{C_v}\,(\nabla\cdot\mathbf{v}) = \frac{Q}{C_v\,e^r} \tag{2}$$

$$\frac{dq}{dt} + \frac{C_p}{C_v}\,(\nabla\cdot\mathbf{v}) = \frac{Q}{C_v\,e^r} \tag{3}$$

where R is the gas constant for dry air, C_p the specific heat capacity of dry air at constant pressure, C_v the specific heat capacity of dry air at constant volume, $\mathbf{F}(t,x,z)$ is the diabatic momentum forcing, $Q(t,x,z)$ the heat per unit mass and unit time added to the air, $\phi(z) = gz$ the geopotential, $\nabla\phi$ the gradient of geopotential, ∇q the gradient of the logarithm of pressure and $\nabla\cdot\mathbf{v}$ the divergence of the velocity.

The spatial domain of the model when described in Cartesian coordinates (x,z) is bounded by a rigid top at $z = H_T$ and a rigid bottom at $z = H_B(x)$. The original Cartesian coordinates (x,z) are transformed into (X,Z), model coordinates hereafter, where the new vertical coordinate is chosen such that the bottom and top boundaries are $Z = 0$ and $Z = 1$ respectively. A general hybrid vertical coordinate based on height can be used such that the coordinate

transformation is written as

$$x(X, Z) = X \tag{4}$$

$$z(X, Z) = \psi(X, Z) \tag{5}$$

where $\psi(X, Z)$ is a function which satisfies the boundary conditions $\psi(X, 0) = H_B(X)$ and $\psi(X, 1) = H_T$. A global invertibility condition is also required, so that the transformation from (x, z) to (X, Z) is bijective. A possible choice is the Gal-Chen vertical coordinate (Gal-Chen, 1975)

$$\psi(X, Z) = H_T Z + H_B(X)(1 - Z) \tag{6}$$

A better possible choice is the set of height based hybrid coordinates presented in (Schär, 2002) which has an exponential vertical decay of the terrain structure. In the simplest case, used here, it is

$$\psi(X, Z) = H_T Z + H_B(X) \frac{\sinh(\gamma(1 - Z))}{\sinh(\gamma)} \tag{7}$$

One of the aims of this work is to explore the use of a fully coordinate-independent formulation of the Euler Equations in the context of a numerical simulation. This includes the use of contravariant components of the velocity as prognostic variables, in contrast to the generalized use of the velocity components expressed in a local Cartesian basis. The prognostic variables are of two types: the scalars r and q which do not change under a coordinate transformation, and the velocity which is a contravariant vector and then its components change from (u, w) in the Cartesian coordinates to (U, W) in the model coordinates. The results from the Riemannian Geometry theory (for instance, Christian Bär, 2010) can be applied to find the expression of the Euler Equations in the model coordinates. Care must be taken to find the expressions of the differential operators which are present in the Euler equations (1) to (3). Following the Riemannian Geometry theory, the first step is to find the expression of

the metric tensor $G_{XZ} = J^T\, G_{xz}\, J$ in the new coordinates

$$G_{XZ} = \begin{pmatrix} 1+\psi_X^2 & \psi_X\psi_Z \\ \psi_X\psi_Z & \psi_Z^2 \end{pmatrix} \tag{8}$$

where G_{xz} is the metric tensor of the Euclidean space in the Cartesian coordinates, which is the identity, and J is the Jacobian matrix of the coordinate transformation

$$J = \begin{pmatrix} 1 & 0 \\ \psi_X & \psi_Z \end{pmatrix} \tag{9}$$

where ψ_X and ψ_Z are the partial derivatives of ψ in the X and Z directions. The metric given in the model coordinates (8) is non orthogonal, except in the case $\psi_X = 0$, that is, where the terrain is flat. The determinant of the metric tensor, which is needed in the calculation of the divergence, is ψ_Z^2.

The introduction of the model coordinates is useful not only because the boundaries are easily defined in this coordinates, but also because the free slip conditions for the contravariant velocity components are very simple expressions, as it is demonstrated in the following. The relation between the contravariant components of the velocity vector in the two set of coordinates and are

$$\begin{pmatrix} U \\ W \end{pmatrix} = J^{-1} \begin{pmatrix} u \\ w \end{pmatrix} = \begin{pmatrix} u \\ \psi_Z^{-1}(w - \psi_X u) \end{pmatrix} \tag{10}$$

The free slip lower boundary condition in the Cartesian coordinates is

$$w(t,x,z) - H_B'(x)\, u(t,x,z) = 0 \tag{11}$$

at $z = H_B(x)$ where $H_B'(X)$ is the derivative of $H_B(X)$ with respect to X. In terms of the velocity components in the model coordinates this free slip boundary condition is $W(t,X,Z) = 0$ at $Z = 0$, because at the lower boundary $\psi(X,0) = H_B(X)$ and then the free slip condition is equivalent to $w - \psi_X u = 0$. Similarly, at the upper boundary the free

slip condition $w(t,x,z)=0$ at $z=H_T$ is $W(t,X,Z)=0$ at $Z=1$. Therefore, the free slip boundary conditions are equivalent to impose $W=0$ at the lower and upper boundaries, a trivial expression that simplifies the task of its implementation.

The contravariant form of the gradient operator applied to $q(t,X,Z)$ is

$$(\nabla q)^X = \left(G^{XX}\frac{\partial}{\partial X} + G^{XZ}\frac{\partial}{\partial Z} \right) q \tag{12}$$

$$(\nabla q)^Z = \left(G^{ZX}\frac{\partial}{\partial X} + G^{ZZ}\frac{\partial}{\partial Z} \right) q \tag{13}$$

where G^{XZ} is the inverse of the metric tensor. The gradient of the geopotential present in the momentum equation can be simplified a lot because $\phi(X,Z)=g\psi(X,Z)$ and then

$$(\nabla \phi)^X = \left(\frac{\partial}{\partial X} - \frac{\psi_X}{\psi_Z}\frac{\partial}{\partial Z} \right) g\psi = 0 \tag{14}$$

$$(\nabla \phi)^Z = \left(-\frac{\psi_X}{\psi_Z}\frac{\partial}{\partial X} + \frac{1+\psi_X^2}{\psi_Z^2}\frac{\partial}{\partial Z} \right) g\psi = \frac{g}{\psi_Z} \tag{15}$$

The divergence of the contravariant velocity vector is, recalling that the determinant of the metric is ψ_Z^2

$$\nabla \cdot \mathbf{V} = \frac{1}{\psi_Z}\left(\frac{\partial}{\partial X}(\psi_Z U) + \frac{\partial}{\partial Z}(\psi_Z W) \right) \tag{16}$$

The advection term in the momentum equation is expressed as the covariant derivative of the velocity field in the direction given by the velocity field itself, written as $\nabla_{\mathbf{V}}\mathbf{V}$. The non-zero Christoffel Symbols of the G_{XZ} metric tensor are

$$\Gamma^Z_{XX} = \frac{\psi_{XX}}{\psi_Z} \tag{17}$$

$$\Gamma^Z_{XZ} = \frac{\psi_{XZ}}{\psi_Z} = \Gamma^Z_{ZX} \tag{18}$$

$$\Gamma^Z_{ZZ} = \frac{\psi_{ZZ}}{\psi_Z} \tag{19}$$

and the two components of $\nabla_{\mathbf{V}}\mathbf{V}$ are

$$(\nabla_{\mathbf{V}}\mathbf{V})^X = \left(U\frac{\partial U}{\partial X} + W\frac{\partial U}{\partial Z}\right) \tag{20}$$

$$(\nabla_{\mathbf{V}}\mathbf{V})^Z = \left(U\frac{\partial W}{\partial X} + W\frac{\partial W}{\partial Z}\right) + \frac{\psi_{XX}}{\psi_Z}U^2 + 2\frac{\psi_{XZ}}{\psi_Z}UW + \frac{\psi_{ZZ}}{\psi_Z}W^2 \tag{21}$$

Finally, the contravariant Euler Equations are

$$\frac{\partial U}{\partial t} + (\nabla_{\mathbf{V}}\mathbf{V})^X + Re^r\left(\frac{\partial q}{\partial X} - \frac{\psi_X}{\psi_Z}\frac{\partial q}{\partial Z}\right) = F_U \tag{22}$$

$$\frac{\partial W}{\partial t} + (\nabla_{\mathbf{V}}\mathbf{V})^Z + Re^r\left(\frac{1+\psi_X^2}{\psi_Z^2}\frac{\partial q}{\partial Z} - \frac{\psi_X}{\psi_Z}\frac{\partial q}{\partial X}\right) + \frac{g}{\psi_Z} = F_W \tag{23}$$

$$\frac{\partial r}{\partial t} + \left(U\frac{\partial r}{\partial X} + W\frac{\partial r}{\partial Z}\right) + \frac{R}{C_v}(\nabla\cdot\mathbf{V}) = \frac{Q}{C_v} \tag{24}$$

$$\frac{\partial q}{\partial t} + \left(U\frac{\partial q}{\partial X} + W\frac{\partial q}{\partial Z}\right) + \frac{C_p}{C_v}(\nabla\cdot\mathbf{V}) = \frac{Q}{C_v} \tag{25}$$

where the divergence is given in (16) and the advection terms for the velocity are given in equations (20) and (21). In the case of a simulation on the sphere the procedure followed here would be also valid, although the calculation of the metric tensor and Christoffel symbols are more costly.

3 Time discretization

The classical three time level (3TL) semi-implicit scheme (Robert, 1981) is used. Although the 3TL scheme has the disadvantage of having a computational mode, it is easier to implement than the two time level scheme and the numerical instability that comes from the computational mode can be avoided by using an Asselin time filter (Asselin, 1972). The atmosphere at each time step $t_n = n\Delta t$ is represented by a vector function X_n which contains the values of velocity, and logarithms of pressure and temperature. The time derivative of the atmosphere state at time t_n is approximated as the difference $X_{n+1} - X_{n-1}$ divided by the time interval $2\Delta t$. This approximation is centered and second order accurate in time. On the other hand, the forcing term to the atmosphere state X_n is represented by $M(X_n)$.

Because the presence of high frequency waves in the solution of the Euler equations if the time stepping is explicit the model should run with very small time steps to avoid numerical instability, and the computational cost would be very high for numerical weather prediction. To solve this problem the semi-implicit technique will be applied. We followed the same time discretization described in (Bubnová et al., 1995). Therefore, it is necessary to find a linear version $L(X_n)$ of $M(X_n)$ around an isothermal atmosphere in hydrostatic balance at rest horizontally uniform. The forcing terms are replaced by the sum of an explicit non linear term $M(X_n) - L(X_n)$ plus value of the linear model applied to an average of the values of the atmospheric state at the previous and the next time steps, X_{n-1} and X_{n+1} respectively. A decentering factor ϵ can be used to increase the damping of the highest frequency waves, being the scheme second order in time when $\epsilon = 0$. Then, the 3TL level scheme is represented by the following equation

$$\frac{X_{n+1} - X_{n-1}}{2\Delta t} = M(X_n) - L(X_n) + \frac{1-\epsilon}{2} L(X_{n-1}) + \frac{1+\epsilon}{2} L(X_{n+1}) \tag{26}$$

From this equation

$$X_{n+1} = (1 - \Delta t\,(1+\epsilon)L)^{-1}\, R(X_{n-1}, X_n) \tag{27}$$

where

$$R(X_{n-1}, X_n) = X_{n-1} + 2\Delta t M(X_n) - \Delta t L\,(2X_n - (1-\epsilon)X_{n-1}) \tag{28}$$

The reference state is an isothermal atmosphere at temperature e^{r^*} in hydrostatic balance at rest. The linear metric terms are derived from a linear metric G^*_{XZ}, which is obtained from a reference coordinate transformation based on a function $\psi^*(Z)$ which do not depend on X and that is calculated from $\psi(X, Z)$ using the constant orography $H^*_B(x) = 0$. This is similar to the use of a constant hydrostatic pressure at surface when the vertical coordinate is the mass based coordinate. For the Gal-Chen (Gal-Chen, 1975) and the set of vertical hybrid coordinates reported in (Schär, 2002) $\psi^*(Z)$ is simply $\psi^*(Z) = ZH_T$ and its derivatives are

$\psi_X^* = 0$ and $\psi_Z^* = H_T$. The linear metric tensor is

$$G_{XZ}^* = \begin{pmatrix} 1 & 0 \\ 0 & H_T^2 \end{pmatrix} \tag{29}$$

The reference state is hydrostatic and then

$$\frac{\partial q^*}{\partial Z} = -\frac{g H_T}{R e^{r*}} \tag{30}$$

When linearising the model it must be taken into account than the reference value $q^*(Z)$ depends linearly on the vertical coordinate Z and then the derivative $q_Z^*(Z)$ is a non zero constant. As a consequence, in the vertical momentum equation there is a linear term in r and in the prognostic equation for q there is a term corresponding to the vertical advection of the reference value q^*. The linear equations corresponding to the non linear model given in (22) to (25) are

$$\frac{\partial U}{\partial t} + R e^{r*} \frac{\partial q}{\partial X} = 0 \tag{31}$$

$$\frac{\partial W}{\partial t} + \frac{R e^{r*}}{H_T^2} \frac{\partial q}{\partial Z} - \frac{g}{H_T} r = 0 \tag{32}$$

$$\frac{\partial r}{\partial t} + \frac{R}{C_v} \left(\frac{\partial U}{\partial X} + \frac{\partial W}{\partial Z} \right) = 0 \tag{33}$$

$$\frac{\partial q}{\partial t} + \frac{C_p}{C_v} \left(\frac{\partial U}{\partial X} + \frac{\partial W}{\partial Z} \right) - \frac{H_T g}{R e^{r*}} W = 0 \tag{34}$$

After the time discretization using the 3TL semi-implicit scheme given in equations (27) and (28) the linear system of equations (31) to (34) is transformed to

$$U_{n+1} + \beta R e^{r^*} \frac{\partial q_{n+1}}{\partial X} = R_U \tag{35}$$

$$W_{n+1} + \beta \left(\frac{R\, e^{r^*}}{H_T^2} \frac{\partial q_{n+1}}{\partial Z} - \frac{g}{H_T} r_{n+1} \right) = R_W \tag{36}$$

$$r_{n+1} + \beta \frac{R}{C_v} \left(\frac{\partial U_{n+1}}{\partial X} + \frac{\partial W_{n+1}}{\partial Z} \right) = R_r \tag{37}$$

$$q_{n+1} + \beta \left(\frac{C_p}{C_v} \left(\frac{\partial U_{n+1}}{\partial X} + \frac{\partial W_{n+1}}{\partial Z} \right) - \frac{H_T g}{R e^{r^*}} W_{n+1} \right) = R_q \tag{38}$$

where $\beta = \Delta t(1+\epsilon)$ and R_U, R_W, R_r and R_q are the explicit terms in (28).

4 Space discretization

All the variables in the model are defined at the same grid of points located at (X_i, Z_j) where i ranges from 1 to N_X and j from 1 to N_Z, being N_X and N_Z the horizontal and vertical dimensions of the grid.

It has not been considered staggering the variables in the horizontal nor in the vertical. The choice of not staggering the variables in the vertical was made because our interest was to develop a vertical finite element (VFE) scheme, where all the variables are set at the same full levels, as in the VFE implementation at the ECMWF IFS model hydrostatic model (Untch and Hortal, 2004). In the horizontal the discretization is spectral and therefore staggered should not be used either.

The distance between consecutive values of X_i is constant in order to apply the Fast Fourier Transform method (FFT) and the distance between consecutive Z_j is variable to permit more density of levels where it is necessary, for instance, near the lower boundary. Any field $f(X,Z)$ is defined by a set of real numbers f^{ij} which represents the value of the field around each grid point. The set of numbers f^{ij} is a discrete representation of a continuous field and can be represented by a $(N_X \times N_Z)$ matrix $\mathbf{f}$ (the bold characters are used to represent different arrays used in the model). The derivative operators respect to X and Z are linear operators acting over the space of discrete fields, and are represented by the square matrices $\mathbf{D_X}$ $(N_X \times N_X)$ and $\mathbf{D_Z}$ $(N_Z \times N_Z)$. The horizontal derivative acts over each row of the discrete field whereas the vertical derivative acts over each column. More precisely, the result of applying the horizontal derivative $\mathbf{D_X}$ on a discrete field $\mathbf{f}$ is the field $\mathbf{D_X} \cdot \mathbf{f}$ defined by the expression

$$(\mathbf{D_X} \cdot \mathbf{f})^{ij} = \sum_{k=1,N_X} D_X^{ik} f^{kj} \tag{39}$$

and similarly the vertical derivative $\mathbf{D_Z}$ applied on a discrete field $\mathbf{f}$ is the field

$$(\mathbf{D_Z} \cdot \mathbf{f})^{ij} = \sum_{k=1,N_Z} D_Z^{jk} \, f^{ik} \tag{40}$$

As a consequence of the above definitions the horizontal and vertical derivatives commute, $\mathbf{D_X} \cdot \mathbf{D_Z} \cdot \mathbf{f} = \mathbf{D_Z} \cdot \mathbf{D_X} \cdot \mathbf{f}$. All the horizontal derivatives are spectral and then the operator $\mathbf{D_X}$ involves the Discrete Fourier Transform and its inverse (the FFT algorithm is used). The vertical derivative matrix $\mathbf{D_Z}$ will be constructed here using the finite elements technique.

The vertical discretization is simple. As already mentioned, all the variables are located at full levels. However, the contravariant vertical velocity W has two more levels located at the very top and bottom of the domain (at Z equal 0 and 1) where the vertical velocity has the boundary value $W = 0$. This implies that an additional vertical derivative operator must be defined, to take into account that the boundary values of the vertical velocity are set to $W = 0$ at the extended levels located at the top and bottom of the domain. Let be $\hat{\mathbf{D}}_\mathbf{Z}$ this special vertical derivative. After the spatial discretization the linear system of equations (35) to (38) is transformed to

$$\mathbf{d}_{n+1} + \beta Re^{r^*} \mathbf{D}_\mathbf{X}^2 \, \mathbf{q}_{n+1} = \mathbf{D_X} \, \mathbf{R}_U \tag{41}$$

$$\mathbf{W}_{n+1} + \beta \left(\frac{Re^{r^*}}{H_T^2} \, \mathbf{D_Z} \, \mathbf{q}_{n+1} - \frac{g}{H_T} \mathbf{r}_{n+1} \right) = \mathbf{R}_W \tag{42}$$

$$\mathbf{r}_{n+1} + \beta \frac{R}{C_v} \left(\mathbf{d}_{n+1} + \hat{\mathbf{D}}_\mathbf{Z} \, \mathbf{W}_{n+1} \right) = \mathbf{R}_r \tag{43}$$

$$\mathbf{q}_{n+1} + \beta \left(\frac{C_p}{C_v} \left(\mathbf{d}_{n+1} + \hat{\mathbf{D}}_\mathbf{Z} \, \mathbf{W}_{n+1} \right) - \frac{H_T g}{Re^{r^*}} \mathbf{W}_{n+1} \right) = \mathbf{R}_q \tag{44}$$

where the horizontal divergence to the horizontal momentum equation has been applied. The unknown horizontal velocity $\mathbf{U}_{n+1}$ has been replaced by the unknown horizontal divergence, $\mathbf{d}_{n+1} = \mathbf{D_X} \, \mathbf{U}_{n+1}$. In the process of solving the linear system the following constants are

used

$$c_*^2 = \frac{C_p}{C_v} R T^* \tag{45}$$

$$N_*^2 = \frac{g^2}{C_p T^*} \tag{46}$$

$$H_* = \frac{R T^*}{g} \tag{47}$$

The procedure is to substitute $\mathbf{r}_{n+1}$ and $\mathbf{q}_{n+1}$ from equations (43) and (44) into equations (41) and (42). Equation (41) can be written as

$$\mathbf{A}_{dd}\,\mathbf{d}_{n+1} + \mathbf{A}_{dW}\,\mathbf{W}_{n+1} = \mathbf{B}_d \tag{48}$$

where

$$\mathbf{A}_{dd} = 1 - \beta^2 c_*^2\,\mathbf{D}_{\mathbf{X}}^2 \tag{49}$$

$$\mathbf{A}_{dW} = \beta^2\,\mathbf{D}_{\mathbf{X}}^2 \left(H_T g - c_*^2\,\hat{\mathbf{D}}_{\mathbf{Z}} \right) \tag{50}$$

$$\mathbf{B}_d = \mathbf{D}_{\mathbf{X}}\,\mathbf{R}_U - \beta R\, e^{r^*}\,\mathbf{D}_{\mathbf{X}}^2\,\mathbf{R}_q \tag{51}$$

and equation (42) can be written as

$$\mathbf{A}_{Wd}\,\mathbf{d}_{n+1} + \mathbf{A}_{WW}\,\mathbf{W}_{n+1} = \mathbf{B}_W \tag{52}$$

where

$$\mathbf{A}_{Wd} = \beta^2 \left(\frac{gR}{H_T C_v} - \frac{c_*^2}{H_T^2}\,\mathbf{D}_{\mathbf{Z}} \right) \tag{53}$$

$$\mathbf{A}_{WW} = 1 - \beta^2 \left(-\frac{g}{H_T} \left(\mathbf{D}_{\mathbf{Z}} + \frac{R}{C_v} \hat{\mathbf{D}}_{\mathbf{Z}} \right) + \frac{c_*^2}{H_T^2}\,\mathbf{D}_{\mathbf{Z}}\,\hat{\mathbf{D}}_{\mathbf{Z}} \right) \tag{54}$$

$$\mathbf{B}_W = \mathbf{R}_W - \beta \left(\frac{R e^{r^*}}{H_T^2}\,\mathbf{D}_{\mathbf{Z}}\,\mathbf{R}_q - \frac{g}{H_T} \mathbf{R}_r \right) \tag{55}$$

The unknown variables are reduced to $\mathbf{d}_{n+1}$ and $\mathbf{W}_{n+1}$ in equations (48) and (52), and due to the commutative property $\mathbf{A}_{Wd}\,\mathbf{A}_{dd} = \mathbf{A}_{dd}\,\mathbf{A}_{Wd}$ the system is reduced to the vertical

velocity $\mathbf{W}_{n+1}$ and can be solved. The equation for $\mathbf{W}_{n+1}$ is

$$(\mathbf{A}_{dd}\mathbf{A}_{WW} - \mathbf{A}_{Wd}\mathbf{A}_{dW})\,\mathbf{W}_{n+1} = \mathbf{A}_{dd}\,\mathbf{B}_W - \mathbf{A}_{Wd}\,\mathbf{B}_d = \mathbf{R}_C \tag{56}$$

After some simplifications the following structure equation is obtained, which is similar to the structure equation of the ALADIN model (Bubnová et al., 1995)

$$\left(\mathbf{I} - \beta^2 c_*^2 \left(\mathbf{D}_{\mathbf{X}}^2 + \mathbf{L}_{\mathbf{Z}}\right) - \beta^4 c_*^2 N_*^2\, \mathbf{D}_{\mathbf{X}}^2\right)\, \mathbf{W}_{n+1} = \mathbf{R}_C \tag{57}$$

where the vertical Laplacian $\mathbf{L}_{\mathbf{Z}}$ is

$$\mathbf{L}_{\mathbf{Z}} = \frac{1}{H_*^2}\left(\left(\frac{H_*}{H_T}\right)^2 \mathbf{D}_{\mathbf{Z}}\hat{\mathbf{D}}_{\mathbf{Z}} - \left(\frac{H_*}{H_T}\right)\hat{\mathbf{D}}_{\mathbf{Z}}\right) \tag{58}$$

The constant matrix $\mathbf{L}_{\mathbf{Z}}$ depends only on the reference temperature and the locations of the vertical levels. This makes the solver efficient because the diagonalization is done once at the set up of the model run. Because in equation (57) the eigenvalues of the $-\mathbf{D}_{\mathbf{X}}^2$ operator are real non-negative, the matrix $-\mathbf{L}_{\mathbf{Z}}$ must have also real non-negative eigenvalues for achieving stability. This condition can be achieved easily for a wide range of vertical levels positions and reference atmosphere values.

Projecting equation (57) on the horizontal spectral space and on the eigenvectors of the vertical matrix $\mathbf{L}_{\mathbf{Z}}$ we obtain a set of independent scalar equations, which are trivially solved.

Once the values of the vertical velocity at the next time step are found from (57) the values of the divergence $\mathbf{d}_{n+1}$ are obtained from equation (48) and $\mathbf{r}_{n+1}$ and $\mathbf{q}_{n+1}$ from (43) and (44) respectively. The values of the horizontal velocity are found from the equation (41), before the horizontal divergence was applied

$$\mathbf{U}_{n+1} = \mathbf{R}_U - \beta Re^{r^*}\mathbf{D}_{\mathbf{X}}\,\mathbf{q}_{n+1} \tag{59}$$

5 Vertical operators

The vertical levels of the model are defined by a set of N_Z real values of the vertical coordinate, Z_1 to Z_{N_Z}, plus the bottom and top levels which are placed at $Z_0 = 0$ and $Z_{N_Z+1} = 1$ respectively which represents the lower and upper boundaries of the spatial domain. At least, three vertical operators must be discretized, the vertical derivative of a function without boundary conditions, $\mathbf{D_Z}$, and the first and second vertical derivative of a function that is zero at the boundaries, $\hat{\mathbf{D}}_\mathbf{Z}$ and $\mathbf{D_Z}\hat{\mathbf{D}}_\mathbf{Z}$ respectively. The operator $\mathbf{D_Z}$ is used for any field except for the the contravariant vertical velocity for which $\hat{\mathbf{D}}_\mathbf{Z}$ is used instead. The operator $\mathbf{D_Z}\hat{\mathbf{D}}_\mathbf{Z}$ is only used in the vertical Laplacian in equation (58).

In orded to have a unified nomenclature for the vertical operators we denote by $\mathbf{D}_\mathbf{Z}^{(\mathbf{i})}$ the first derivative operator applied to a discrete function $\mathbf{f}$ that has zero (i) derivative at the boundaries. Similarly, $\mathbf{S}_\mathbf{Z}^{(\mathbf{i})}$ denotes the second derivative operator applied to a discrete function with the same boundary conditions as $\mathbf{D}_\mathbf{Z}^{(\mathbf{i})}$. Therefore, $\mathbf{S}_\mathbf{Z}^{(\mathbf{0})}$ is used for the vertical Laplacian and $\mathbf{S}_\mathbf{Z}^{(\mathbf{1})}$ for the diffusion operator, which is applied to a function that has zero first derivative at the boundaries and will be used in some of the tests in section 8. To unify the method of construction of the operators all the discrete functions are supposed to have some condition at the boundaries. In the case of a function without any boundary conditions, the first derivative operator used when using a cubic spline representation will be $\mathbf{D}_\mathbf{Z}^{(\mathbf{3})}$ and if it were necessary $\mathbf{S}_\mathbf{Z}^{(\mathbf{3})}$ should be used for the second derivative.

The VFE scheme used here is similar to the IFS implementation (Untch and Hortal, 2004) although there are differences, mainly in the domain of the cubic B-splines, the position of the breakpoints and the treatment of the boundaries.

The domain of the B-splines is the closed interval Z_0 to Z_{N_Z+1}. A number of B-splines from $\mathcal{B}_0(Z)$ to $\mathcal{B}_{N_Z+1}(Z)$ are calculated following the recursive de Boor Algorithm (de Boor, 2001) by imposing continuity of the splines up to the second derivative at a set of breakpoints. Under this conditions, the number of breakpoints to get $N_Z + 2$ splines is N_Z. Therefore there is some degree of freedom to select which set of breakpoints are going to be used. The

configuration shown here is not unique, but it provides good results in the cases that have been explored. All model levels except levels 1 and 2 near the lower boundary, and levels $N_Z - 1$ and N_Z near the upper boundary have been selected to be breakpoints. To complete the set of N_Z breakpoints, two more breakpoints, b_1 and b_2, are located at positions

$$b_1 = (1 - \alpha)\, Z_0 + \alpha Z_3 \tag{60}$$

$$b_2 = (1 - \alpha)\, Z_{N_Z+1} + \alpha Z_{N_Z-2} \tag{61}$$

where the parameter α is selected to optimize stability in a set of test cases. The value $\alpha = 0.5$ is used in all the results presented here.

So far, the set of breakpoints permits to define the B-splines basis functions $\mathcal{B}_0(Z)$ to $\mathcal{B}_{N_Z+1}(Z)$, that is, piecewise cubic polynomials which are continuous up to the second derivative at the breakpoints. Any discrete function $\mathbf{f}$ defined at each model level consists of a vector of N_Z real numbers f_1 to f_{N_Z}. This function can be represented as cubic polynomial $f(Z)$ which is a linear combination of the B-splines basis functions

$$f(Z) = \sum_{j=0,N_Z+1} \hat{f}_j\, \mathcal{B}_j(Z) \tag{62}$$

where the coefficients $\hat{f}_j$ are determined from the N_Z conditions $f_j = f(Z_j)$ and the boundary conditions $f^{(i)}(0) = 0$ and $f^{(i)}(1) = 0$ where (i) depends on the operator being discretized as mentioned above. The inverse transform, that is, the computation of the value of a discrete function from the spline space representation is done using the value of the spline at each model level, $f_j = f(Z_j)$.

This can be put in matrix form as $\hat{\mathbf{f}} = \mathbf{A^{(i)}}\, \mathbf{f}$ and $\mathbf{f} = \mathbf{B^{(i)}}\, \hat{\mathbf{f}}$. Matrix $\mathbf{A^{(i)}}$ maps a discrete function from the physical space, represented by the vector $\mathbf{f}$, to the spline space, represented by the vector $\hat{\mathbf{f}}$, taking into account that the boundary conditions are applied in the spline space representation. Matrix $\mathbf{B^{(i)}}$ do the inverse, maps a discrete function from the spline space, represented by the vector $\hat{\mathbf{f}}$, to the physical space, represented by the vector $\mathbf{f}$.

Following (Untch and Hortal, 2004) the Garlekin method is applied in the spline space.

Figure 1: Numerical error of the discrete vertical derivative $\hat{\mathbf{D}}_{\mathbf{Z}}$ for the test function $f(Z) = \sin(6\pi Z)$, $f'(Z) = 6\pi\cos(6\pi Z)$. Error in blue, analytical value in green. The number of levels is 40, from 0.0125 to 0.9875 at a constant distance $\Delta Z = 0.0250$.

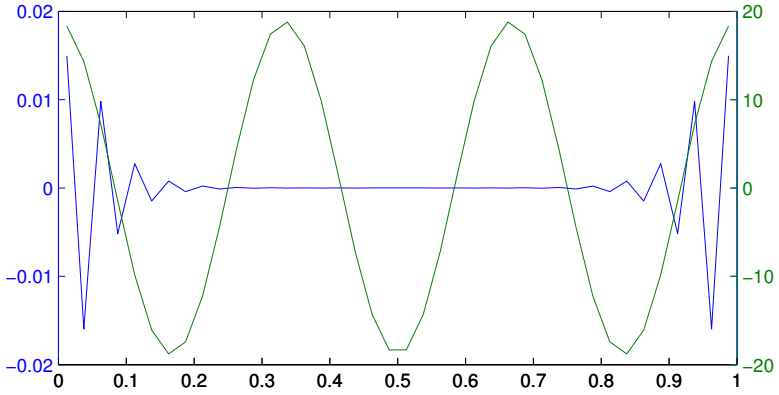

The discrete vertical derivative operator with boundary conditions $\mathbf{D}_{\mathbf{Z}}^{(\mathbf{i})}$ is represented by the matrix $\mathbf{B}^{(\mathbf{i})}\,\mathbf{M}^{-1}\,\mathbf{D}\,\mathbf{A}^{(\mathbf{i})}$ where

$$M_{ij} = \int_{Z_0}^{Z_{N_Z+1}} \mathcal{B}_i(Z)\,\mathcal{B}_j(Z)\,dZ \tag{63}$$

$$D_{ij} = \int_{Z_0}^{Z_{N_Z+1}} \mathcal{B}_i(Z)\,\frac{\partial \mathcal{B}_j}{\partial Z}(Z)\,dZ \tag{64}$$

Any other vertical linear operator is calculated similarly, consequently changing the operator in equation (64). In particular, the above mentioned second derivative operator with boundary conditions $\mathbf{S}_{\mathbf{Z}}^{(\mathbf{i})}$ is represented by the matrix $\mathbf{B}^{(\mathbf{i})}\,\mathbf{M}^{-1}\,\mathbf{S}\,\mathbf{A}^{(\mathbf{i})}$ where

$$S_{ij} = \int_{Z_0}^{Z_{N_Z+1}} \mathcal{B}_i(Z)\,\frac{\partial^2 \mathcal{B}_j}{\partial Z^2}(Z)\,dZ \tag{65}$$

The numerical error of the discrete vertical derivative $\mathbf{D}_{\mathbf{Z}}^{(\mathbf{1})}$ for the test function $f(Z) = \sin(6\pi Z)$ is plotted in figure (1). The discrete second vertical derivative $\mathbf{S}_{\mathbf{Z}}^{(\mathbf{1})}$ is applied to the same test function and the numerical error is plotted in figure (2). In both cases, the number of levels is 40, from 0.0125 to 0.9875 at a constant interval of $\Delta Z = 0.0250$.

Figure 2: Numerical error of the discrete vertical derivative $\mathbf{D_Z}\hat{\mathbf{D}}_\mathbf{Z}$ for the test function $f(Z) = \sin(6\pi Z)$, $f''(Z) = -(6\pi)^2 \sin(6\pi Z)$. Error in blue, analytical value in green. The number of levels is 40, from 0.0125 to 0.9875 at a constant distance $\Delta Z = 0.0250$.

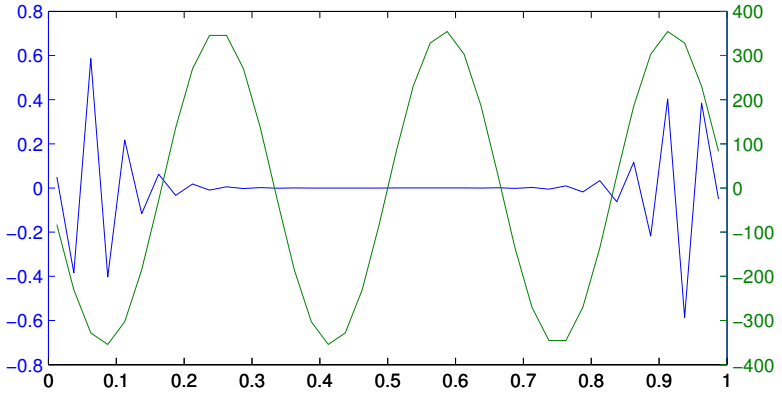

6 Semi-Lagrangian advection

In this section a covariant semi-Lagrangian scheme, in the sense that can be used in any coordinate system using only covariant objects, is presented. It is applied to the present model coordinates and covariant variables. The concepts of parallel transport and geodesic curve, taken from the Differential Geometry (for instance, Christian Bär, 2010) are used for this purpose. Basically, we follow the well known semi-Lagrangian scheme (Robert, 1981; Robert, 1982; Caya and Laprise, 1999; Ritchie et al., 1995) and rewrite the parts that must be changed for achieving covariance.

The parallel transport concept is sometimes implicitly used when we operate with vectors with different base points. This is the case in a semi-Lagrangian scheme, when calculating the difference between the velocity vector at the departure and arrival points. In an Euclidean space the Cartesian coordinates are special in the sense that the parallel transport is the identity, that is, the vector being parallel transported does not change the values of its components. But it is not the case when using a non Cartesian coordinate system, even if the space is Euclidean. To find the semi-Lagrangian trajectory, or the semi-Lagrangian advection of the velocity, we need to calculate the difference between the contravariant velocity vector at the arrival and departure points, and in doing so, we need to do a parallel transport

of the velocity vector from one of them to the other. Given an Euclidean space, a way to do a parallel transport of a vector from the departure point $D = (X_D, Z_D)$ to the arrival point $A = (X_A, Z_A)$ in any coordinate system is to change to the Cartesian basis before and after the parallel translation, that is

$$\begin{pmatrix} U' \\ W' \end{pmatrix} = J^{-1}(A) \cdot J(D) \begin{pmatrix} U \\ W \end{pmatrix} \tag{66}$$

where (U, W) are the velocity components at the departure point and (U', W') are the velocity components after the parallel translation. The Jacobian matrices $J(A)$ and $J(D)$ at the arrival and departure points are used to change the velocity components to the Cartesian basis. In this particular case, the relation between the contravariant components of the velocity vector in the Cartesian and model coordinates at any point P is

$$\begin{pmatrix} u \\ w \end{pmatrix} = J(P) \begin{pmatrix} U \\ W \end{pmatrix} = \begin{pmatrix} 1 & 0 \\ \psi_X(P) & \psi_Z(P) \end{pmatrix} \begin{pmatrix} U \\ W \end{pmatrix} \tag{67}$$

where $J(P)$ is the Jacobian matrix of the coordinate transformation, and ψ_Z, ψ_X the derivatives of $\psi(X, Z)$ respect to X and Z. By substituting the Jacobian (67) into (66) it is found that

$$U' = U \tag{68}$$

$$W' = \frac{\psi_X(D) - \psi_X(A)}{\psi_Z(A)} U + \frac{\psi_Z(D)}{\psi_Z(A)} W \tag{69}$$

It is worth to point out that the horizontal component of the velocity is unchanged after the parallel translation, and only the vertical component is modified. In the case of spherical geometry all components would change.

The trajectory $\mathbf{X}(t) = (X(t), Z(t)) = (X^1(t), X^2(t))$ of a fluid particle follows the

differential equation

$$\frac{d^2X^i(t)}{dt^2} + \Gamma^i_{jk}\left(\mathbf{X}(t)\right)\,\frac{dX^j(t)}{dt}\,\frac{dX^k(t)}{dt} = M^i(\mathbf{X}(t)) \tag{70}$$

where $M^i(\mathbf{X}(t))$ is the contravariant force in the momentum equation (22) and (23), the sum of gradient of pressure, gravity and diabatic forcing. If $M^i(\mathbf{X}(t))$ is omitted then (70) is the geodesic equation, which is a straight line in an Euclidean space. If we know the velocity $\mathbf{V}_P = (U_P, W_P)$ at a point $\mathbf{X}_P$, we can estimate a second order approximation of the trajectory from a simple integration of (70)

$$X^i(t) = X^i_P + V^i_P\,t + \left(M^i(\mathbf{X}_P) - \Gamma^i_{jk}\left(\mathbf{X}_P\right)\,V^j_P\,V^k_P\right)\frac{t^2}{2} + \mathcal{O}(t^3) \tag{71}$$

We suppose that the trajectory begins at the departure point $\mathbf{X}_D$ at time $t - \Delta t$ and ends at the arrival point $\mathbf{X}_A$ at time $t + \Delta t$. The midpoint of the trajectory $\mathbf{X}_M$ at time t can be approximated by the implicit equation

$$X^i_A = X^i_M + V^i_M\,\Delta t + \left(M^i(\mathbf{X}_M) - \Gamma^i_{jk}\left(\mathbf{X}_M\right)\,V^j_M\,V^k_M\right)\frac{\Delta t^2}{2} \tag{72}$$

where $\mathbf{V}_M$ is the contravariant velocity interpolated at the midpoint, and $M^i(\mathbf{X}_M)$ and $\Gamma^i_{jk}\left(\mathbf{X}_M\right)$ are also interpolated values at the midpoint. This equation can be solved by iteration, until enough convergence. A new midpoint $\mathbf{X}_{M'}$ is found from the previous one $\mathbf{X}_M$ from the equation (72)

$$X^i_{M'} = X^i_A - V^i_M\,\Delta t - \left(M^i(\mathbf{X}_M) - \Gamma^i_{jk}\left(\mathbf{X}_M\right)\,V^j_M\,V^k_M\right)\frac{\Delta t^2}{2} \tag{73}$$

and the procedure is repeated until the difference between $\mathbf{X}_{M'}$ and $\mathbf{X}_M$ is small. Once the midpoint is known, the departure point is estimated from (72) doing an backward time integration, that is, replacing Δt with $-\Delta t$

$$X^i_D = X^i_M - V^i_M\,\Delta t + \left(M^i(\mathbf{X}_M) - \Gamma^i_{jk}\left(\mathbf{X}_M\right)\,V^j_M\,V^k_M\right)\frac{\Delta t^2}{2} \tag{74}$$

Finally, from (72) and (74) it is found the departure point

$$X_D^i = X_A^i - V_M^i \, 2\Delta t \tag{75}$$

There are other ways to find the departure point, most of them do not take into account the force term, however the force term has very little influence in the results (not shown). The 3TL scheme in the IFS model (Ritchie et al., 1995) uses the mean of the velocity at the arrival and departure points to calculate the trajectory. This procedure could be applied in a covariant context, if the velocity at the departure point is parallel transported to the arrival point before taking the mean value.

A 3TL semi-implicit Eulerian scheme can be represented by (26). In the semi-Lagrangian scheme this equation is changed to (Caya and Laprise, 1999)

$$\frac{X_{n+1}^A - X_{n-1}^D}{2\Delta t} = \frac{1-\epsilon}{2}\left(M_n^D - L_n^D + L_{n-1}^D\right) + \frac{1+\epsilon}{2}\left(M_n^A - L_n^A + L_{n+1}^A\right) \tag{76}$$

where the superscript A and D indicates that the term is being calculated at the arrival or departure point respectively, and M does not include advection. The variables included in X are the logarithm of pressure and temperature, which are scalars, and the contravariant velocity, which is a vector and therefore must be parallel transported using (66) from departure point D to arrival point A. A similar statement holds for M, therefore, the components corresponding to the velocity equation must be parallel transported. The linear model L uses a simplified geometry, because the orography is omitted in it, and then the velocity components must be parallel transported using the corresponding simplified Jacobian in (66). This simplified Jacobian is same at any point and, therefore, the parallel transport for the linear model is the identity in this case. The use of the full and the linear parallel transport in the same equation is an apparent inconsistency of the semi-implicit scheme, but it must be taken into account that the linear model contribution in (76) cancels when the time step is small, consistently with the idea that the linear model contribution is added only for stability and

efficiency purposes. After reordering the terms of equation (76) we obtain

$$X^A_{n+1} - (1+\epsilon)\Delta t\, L^A_{n+1} = R^A + R^D(G) + R^D(G^*) \tag{77}$$

where $R^D(G)$ and $R^D(G^*)$ are interpolated at the departure point and parallel transported to the arrival point, the first with the complete geometry, the second with the linear geometry. The right hand terms are

$$R^A = (1+\epsilon)\Delta t\, \left(M^A_n - L^A_n\right) \tag{78}$$

$$R^D(G) = X^D_{n-1} + (1-\epsilon)\Delta t\, M^D_n \tag{79}$$

$$R^D(G^*) = (1-\epsilon)\Delta t\, \left(L^D_{n-1} - L^D_n\right) \tag{80}$$

The interpolation is bilinear and it uses the four nearest grid points. Clearly it can be improved to other higher order interpolators, but it has not been done because developing and testing accurate interpolators for a semi-Lagrangian scheme is not the purpose of this work.

In this section it has been demonstrated that a covariant semi-Lagrangian advection can be implemented, and it permits larger time steps than the Eulerian advection, as it is shown if section 8. In this simple implementation the interpolation procedure is bilinear, and can be improved. Results shows that larger time steps produce better results, with less inherent semi-Lagrangian diffusion.

7 Stability

A common technique for doing linear stability analysis of semi-implicit schemes is to replace the non linear model with a linearised model respect to an atmosphere with a reference temperature profile $T^\bullet(Z)$ which is different from the reference temperature T^* used in the semi-implicit linear terms. The residual terms, which appears as soon as both temperatures are different, can lead to instabilities. The stability analysis done in (Bénard, 2003) and

(Bénard et al., 2004) is designed for spatially unbounded dynamical systems that verifies a set of conditions and it is applied to a set of semi-implicit schemes without considering any spatial discretization. In (Bénard, 2003) it is shown that height based coordinate is unstable in the case of vertical propagating acoustic waves, whereas mass based coordinate is stable. In (Bénard et al., 2004) it is shown that height based coordinate is also unstable when considering the full three dimensional set of Euler equations. However, we have found that height based coordinate lead to a stable semi-implicit time stepping in a wide range of cases after considering the spatial vertical discretization. We have not found any reason for this strong differences between the continuous and discrete cases, but the differences are obvious and clear. In this section we follow the linear stability analysis for spatially continuous and unbounded systems described in (Bénard et al., 2004) but for the height vertical coordinate and the prognostic variables used in this work and we complete the stability analysis with a numerical stability analysis method that permits to consider the vertical discretization including the boundary conditions for the vertical velocity.

In the appendix B of (Bénard et al., 2004) there is a stability analysis for the Euler equations using height based vertical coordinate in the framework of spatially continuous and unbounded systems just mentioned above. There the prognostic variables are the same as the model presented here, except that here the temperature is replaced by the logarithm of temperature. Here the stability analysis procedure is identical, but the final result is different, because the choice of prognostic variables has impact on the stability (Bénard et al., 2004). The linear model corresponding to the non linear equations (22) to (25) for a given eigenmode of the horizontal Laplacian operator $-k^2$ can be expressed as

$$\frac{\partial d}{\partial t} = k^2 Re^{r^\bullet} q \tag{81}$$

$$\frac{\partial W}{\partial t} = \frac{g}{H_T} r - \frac{Re^{r^\bullet}}{H_T^2} \frac{\partial q}{\partial Z} \tag{82}$$

$$\frac{\partial r}{\partial t} = -\frac{R}{C_v} \left(d + \frac{\partial W}{\partial Z} \right) - r_Z^\bullet W \tag{83}$$

$$\frac{\partial q}{\partial t} = -\frac{C_p}{C_v} \left(d + \frac{\partial W}{\partial Z} \right) + \frac{H_T g}{Re^{r^\bullet}} W \tag{84}$$

where $r_Z^\bullet$ is the vertical derivative of the logarithm of the reference temperature. We consider $r^\bullet$ constant in the following analysis. The normal modes of the system (81) to (84) are

$$X(Z) = X_0 \exp(ikx) \exp(\mu H_T Z) \tag{85}$$

where X represents the set of prognostic variables and

$$\mu = i\nu + \frac{1}{2H^\bullet} \tag{86}$$

$$H^\bullet = \frac{RT^\bullet}{g} \tag{87}$$

Following the same procedure as in appendix B in (Bénard et al., 2004) we find the following polynomial equation for the growth rate λ

$$\left(\frac{\Lambda_0}{\Delta t}\right)^4 + \left(\frac{\Lambda_0}{\Delta t}\right)^2 c_*^2 \left(\Lambda_1\Lambda_2\left(k^2 + |\mu|^2\right) + \tau\right) + k^2 N_*^2 c_*^2 \Lambda_1^2 \Lambda_2 \Lambda_3 = 0 \tag{88}$$

where

$$\alpha = \frac{T^\bullet}{T^*} - 1 \tag{89}$$

$$\Lambda_0 = \frac{\lambda^2 - 1}{2} \tag{90}$$

$$\Lambda_1 = \frac{\lambda^2 + 1}{2} \tag{91}$$

$$\Lambda_2 = \Lambda_1 + \alpha\lambda \tag{92}$$

$$\Lambda_3 = \Lambda_1 - \frac{\alpha}{1+\alpha}\lambda \tag{93}$$

$$\tau = \frac{\alpha\mu}{4H^\bullet}(\lambda - 1)^2 \left(\lambda^2 + 2\frac{C_v}{C_p}\alpha + 1\right) \tag{94}$$

For long time steps the growth rate is the same as in the mass based coordinate (Bénard et al., 2004) and then the system is equally stable from this point of view. For finite time steps some growth rates have $|\lambda|^2 > 1$ which means that they are not stable. Similarly to the case studied in appendix B of (Bénard et al., 2004) the instabilities are significant when $kH^\bullet \approx \nu H^\bullet \approx 1$.

Figure 3: Maximum module of the amplification matrix eigenvalues Γ for different values of the reference temperature T^*. The horizontal wave numbers selected are the corresponding to a horizontal domain of $N_X = 256$ grid points and a horizontal grid spacing of $\Delta x = 2000\,m$. The time step is $\Delta t = 50\,s$. The decentering parameter is set to $\epsilon = 0.1$. The temperature profile of the explicit linear model is the standard atmosphere.

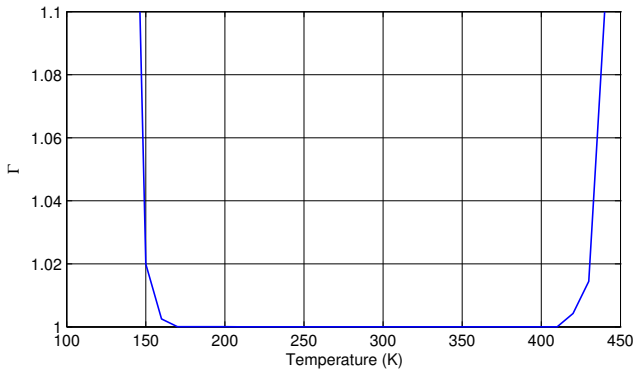

From the fact that the model presented here do not have the instabilities predicted by the continuous analysis just described above, there is no other choice but to proceed to consider the vertical discretization, being the method and results less general. The stability of the 3TL semi-implicit scheme for isothermal and non isothermal bounded linear atmospheric flows can be studied using a numerical analysis method (Côté, Beland and Staniforth, 1983; Bénard et al., 2004). The vertically discretized system (81) to (84) is

$$\frac{\partial \mathbf{d}}{\partial t} = k^2 R T^{\bullet} \mathbf{q} \tag{95}$$

$$\frac{\partial \mathbf{W}}{\partial t} = \frac{g}{H_T}\mathbf{r} - \frac{RT^{\bullet}}{H_T^2}\mathbf{D_Z q} \tag{96}$$

$$\frac{\partial \mathbf{r}}{\partial t} = -\frac{R}{C_v}\left(\mathbf{d} + \hat{\mathbf{D}}_\mathbf{Z}\mathbf{W}\right) - r_Z^{\bullet}\mathbf{W} \tag{97}$$

$$\frac{\partial \mathbf{q}}{\partial t} = -\frac{C_p}{C_v}\left(\mathbf{d} + \hat{\mathbf{D}}_\mathbf{Z}\mathbf{W}\right) + \frac{H_T g}{RT^{\bullet}}\mathbf{W} \tag{98}$$

where $\mathbf{D_Z}$ and $\hat{\mathbf{D}}_\mathbf{Z}$ are the vertical derivative operators and $r_Z^{\bullet}$ is the vertical derivative of the reference logarithm of temperature. It can be written as

$$\frac{\partial \mathbf{X}}{\partial t} = \mathbf{L}^{\bullet}(\mathbf{X}) \tag{99}$$

where $\mathbf{X} = (\mathbf{d}, \mathbf{W}, \mathbf{r}, \mathbf{q})$ is the state vector and $\mathbf{L}^{\bullet}$ is the linear model. The linear model $\mathbf{L}^*$

respect to a given atmosphere with a constant temperature profile T^* is the same, with the difference that $r^\bullet$ is replaced by a constant r^* and therefore $r^*_Z = 0$. For a 3TL centered semi-implicit scheme the model evolution can be written as

$$\mathbf{Y}^{n+1} = \mathbf{A}\left(\mathbf{Y}^{n}\right) \tag{100}$$

where $\mathbf{Y}^{n+1}$ is the generalized state vector defined by $(\mathbf{X}^{n+1}, \mathbf{X}^{n})$ and the amplification matrix $\mathbf{A}$ is

$$\mathbf{A} = \begin{pmatrix} 2\Delta t \left(\mathbf{I} - \Delta t \mathbf{L}^*\right)^{-1} \left(\mathbf{L}^\bullet - \mathbf{L}^*\right) & \left(\mathbf{I} - \Delta t \mathbf{L}^*\right)^{-1} \left(\mathbf{I} + \Delta t \mathbf{L}^*\right) \\ \mathbf{I} & \mathbf{0} \end{pmatrix} \tag{101}$$

where $\mathbf{0}$ and $\mathbf{I}$ are the null and identity operators in the state vector space. A way to construct the amplification matrix is to find each column of $\mathbf{A}$ through the solution of the 3TL semi-implicit scheme given in section 4 replacing there the non linear model with the linear model $\mathbf{L}^\bullet$. The amplification matrix found in this way is not exactly the same as the amplification matrix in equation (101) because in the solution of the linear system described in section 4 the matrix $\mathbf{D_Z}\hat{\mathbf{D}}_\mathbf{Z}$ found in the vertical Laplacian (58) is calculated from a direct discretization of the second derivative operator over a function which is zero at the boundaries, that is the matrix $\mathbf{S}^{(\mathbf{0})}_\mathbf{Z}$ described in section 5, instead of doing the matrix multiplication of the discrete operators $\mathbf{D_Z}$ and $\hat{\mathbf{D}}_\mathbf{Z}$. The results presented in this section are obtained using the solver described in section 4 to find the amplification matrix (101). The numerical stability analysis consists in finding the maximum module of the eigenvalues of the amplification matrix $\mathbf{A}$. If this value is greater than one there is an instability.

The following test has been considered. The horizontal wave numbers selected are the corresponding to a horizontal domain of $N_X = 256$ grid points and a horizontal grid spacing of $\Delta x = 2000\, m$, that corresponds to wave numbers up to $k = 0.0015\, m^{-1}$ approximately. The time step is $\Delta t = 50\, s$. The decentering parameter is set to $\epsilon = 0.1$ in the all numerical stability tests shown, however all the test in section 8 are done with $\epsilon = 0.0$. The reference temperature of the implicit part is $T^* = 350\, K$ and the reference temperature for the explicit

Figure 4: Maximum module of the amplification matrix eigenvalues Γ for different values of the parameter α. The horizontal wave numbers selected are the corresponding to a horizontal domain of $N_X = 256$ grid points and a horizontal grid spacing of $\Delta x = 2000\,m$. The time step is $\Delta t = 50\,s$. The decentering parameter is set to $\epsilon = 0.1$. The reference temperature of the implicit part is $T^* = 350\,K$. In green, the number of vertical levels are 50 with a regular grid spacing and the top of the atmosphere is placed at $30\,km$. In blue, the levels are placed at the geopotential height of the 62 levels of the IFS model when using the standard atmosphere.

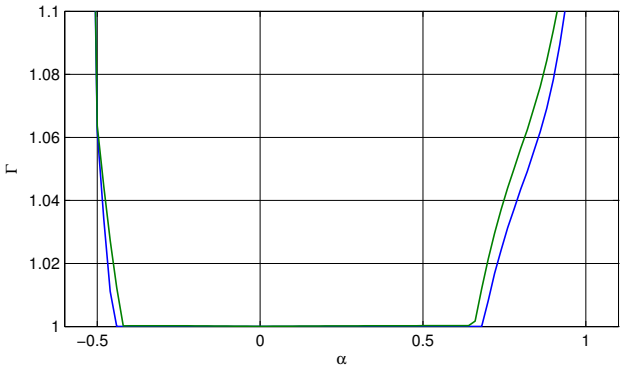

part runs from $T^\bullet = 140\,K$ to $T^* = 735\,K$ at $\Delta T^* = 7K$ intervals, which corresponds to values of the parameter α in the range from -0.6 to 1.1. The test is done for 50 vertical levels with a regular grid spacing and the top of the atmosphere placed at $30\,km$. The same test is repeated for levels placed at the geopotential height of the 62 levels of the IFS model when using the standard atmosphere. The results, plotted in figure (4), shows stability for a wide range of values of the parameter α, from -0.44 to 0.68. The range of stability is greater for the IFS distribution of levels.

Another interesting case is when the temperature profile of the explicit part is not constant (Bénard et al., 2004). We have used the standard atmosphere for $T^\bullet(Z)$, that is, temperature of $288.15\,K$ at surface with a vertical lapse rate of $6.5\,K\,km^{-1}$ and constant temperature over $11\,km$ height. Pressure is calculated from the hydrostatic assumption. The test is similar to the previous one, the number of vertical levels are 50 with a regular grid spacing, the top of the atmosphere is placed at $30\,km$, the time step is $\Delta t = 50\,s$ and the decentering parameter is set to $\epsilon = 0.1$. The reference temperature for the implicit part runs from $T^* = 100\,K$ to $T^* = 450\,K$ at $\Delta T^* = 10K$ intervals. Again, the results plotted in figure (3) shows stability for a wide range of values of the reference temperature.

Figure 5: Vertical and horizontal velocity (ms^{-1}) at $t^* = 120$ with $N = 0.02\,s^{-1}$, $U = 8\,ms^{-1}$, $H_0 = 1\,m$, $a = 16\,km$, $\Delta X = 3.2\,km$ and $H_T\,\Delta Z = 100\,m$. The results are shown for a domain of $14\,km$ height and $384\,km$ width centered at the mountain.

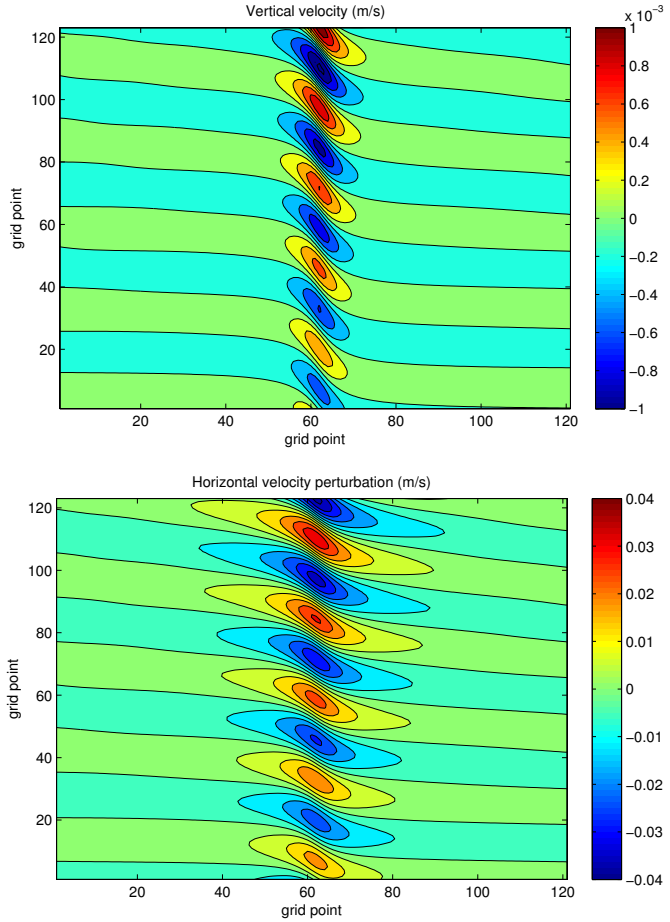

8 Test cases

A set of test cases have been done, all with the same basic configuration. The reference temperature used is $T^* = 350\,K$, the decentering parameter is $\epsilon = 0.0$, the Asselin time filter is 0.10 and the advection is Eulerian, except in the test devoted to the semi-Lagrangian advection. It has not been used any kind of diffusion, except in the warm and cold bubble tests, where an implicit two dimensional diffusion has been applied. The test include hydrostatic and non hydrostatic waves excited by a bell shaped mountain, inertia-gravity excited by a potential temperature perturbation, cold and warm bubble test. More complex orography has been also considered in one of the test.

Figure 6: Vertical and horizontal velocity (ms^{-1}) at $t^* = 90$ with $N = 0.02\,s^{-1}$, $U = 15\,ms^{-1}$, $H_0 = 100\,m$, $a = 500\,m$, $\Delta X = 100\,m$ and $H_T\,\Delta Z = 100\,m$. The results are shown for a domain of $14\,km$ height and $14\,km$ width where the mountain is placed at $3.1\,km$ from the left border of the picture.

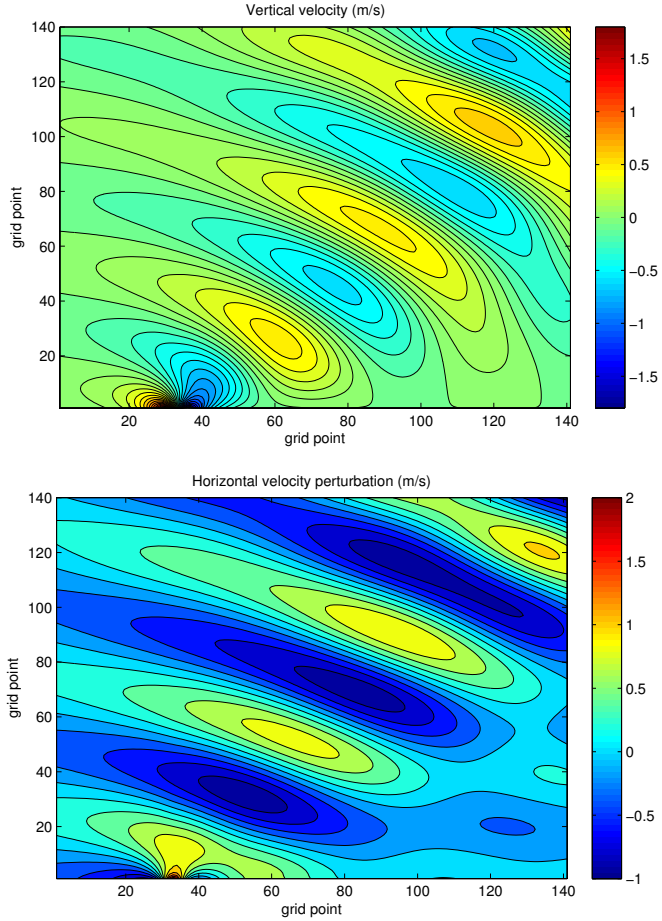

In (Bubnová et al., 1995) a set of idealized tests are described for a 2D flow over a bell shaped mountain with maximum height H_0 and half width a

$$H_B(X) = H_0 \frac{a^2}{a^2 + x^2} \tag{102}$$

The basic flow U and the Brunt-Väisälä frequency N are constant. Four test are described in (Bubnová et al., 1995): hydrostatic linear wave, quasi-linear non hydrostatic wave, potential flow and non linear non hydrostatic flow.

The setting for the hydrostatic linear wave is an isothermal atmosphere with $N = 0.02\,s^{-2}$ and $U = 8\,ms^{-1}$ and the bell shaped mountain has $H_0 = 1\,m$ and $a = 16\,km$. The hori-

zontal and vertical resolutions are $\Delta X = 3.2\,km$ and $H_T\,\Delta Z = 100\,m$ with the top of the atmosphere placed at $H_T = 20\,km$. The absorbing layer begins at $10\,km$. The integration is done up to $t^* = tU/a = 120$ with $\Delta t = 90\,s$. The results for the horizontal velocity perturbation are shown in figure (5) and are very similar to the results in figure 1 of (Bubnová et al., 1995).

The second test selected is also from (Bubnová et al., 1995). It consist on a quasi-linear non hydrostatic wave, with the following changes respect to the previous hydrostatic test: $U = 15\,ms^{-1}$, $H_0 = 100\,m$ and $a = 500\,m$. The horizontal and vertical resolutions are $\Delta X = 100\,m$ and $H_T\,\Delta Z = 100\,m$ with the top of the atmosphere placed at $H_T = 20\,km$.

The absorbing layer begins at $14\,km$. The integration is done up to $t^* = tU/a = 90$ with $\Delta t = 1\,s$. The results are shown in figure (6) for the vertical velocity and horizontal velocity perturbation and are again very similar to the results presented in figures 2 and 3 in (Bubnová et al., 1995).

An interesting test case for considering the response of the model with more complex orography is described in (Schär et al., 2002). The upstream profile is defined by constant value of the Brunt-Väisälä frequency $N = 0.01\,s^{-1}$ and the horizontal velocity $u = 10\,ms^{-1}$ together with the upstream surface temperature $T = 288\,K$ and pressure $p = 1000\,hPa$. The mountain ridge is a bell shaped structure with superposed small scale features

$$H_B(X) = H_0 \exp\left(-\frac{X^2}{a^2}\right) \cos^2\left(\frac{\pi X}{b}\right) \tag{103}$$

where $H_0 = 250\,m$, $a = 5000\,m$ and $b = 4000\,m$.

The gravity waves forced by this mountain have two dominating spectral components: the larger scale is a hydrostatic wave characterized by deep vertical propagation and the smaller scale are generated by the cosine shaped terrain variations and characterized by a rapid decay due to non hydrostatic effects. The vertical resolution is $150\,m$ and the horizontal resolutions is $250\,m$. The number of vertical levels is 130. A Rayleigh damping layer is used over a height of $10.7\,km$ to minimize the reflection of vertically propagating waves at the upper boundary. The time step is $\Delta t = 4\,s$.

Figure 7: Vertical velocity (ms^{-1}) at $t = 40000\,s$ for the Schär test using Eulerian advection. The time step is $\Delta t = 4$, horizontal resolution $\Delta x = 250\,m$ and vertical resolution $H_T\,\Delta Z = 150\,m$.

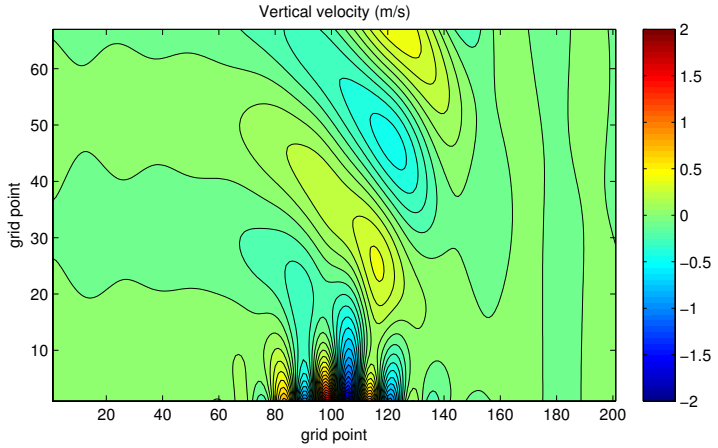

The vertical velocity is shown in figure (7) and it is very similar to the analytical solution given in (Klemp et al., 2003). The covariant semi-Lagrangian advection scheme has been used with the same configuration except that the time step is $\Delta t = 8\,s$. The results, shown in figure (8) are similar to the Eulerian advection case.

The test case found in (Skamarock and Klemp, 1994) is devoted to inertia-gravity waves. There the efficiency and accuracy of the Klemp-Wilhelmson time splitting technique is explored and a propagating inertia-gravity wave is simulated in a Boussinesq atmosphere with constant Brunt-Väisälä frequency in a periodic channel with solid, free-slip upper and lower boundaries. The waves are produced by an initial potential temperature perturbation of the form

$$\theta(X, Z, 0) = \Delta\theta_0 \frac{\sin(\pi Z)}{1 + (X - X_0)^2 / a^2} \tag{104}$$

where a small amplitude $\Delta\theta_0 = 0.01\,K$ is chosen for quantitative comparisons with the analytic solutions of the linearized equations. When the mean flow has a constant horizontal velocity U_0 the linear solutions are (Skamarock and Klemp, 1994)

$$\theta(\hat{X}, Z, t) = \theta(\hat{X}, Z, 0) + \Delta\theta_0 \sin(\pi Z) \int_0^\infty \chi(k, \hat{X})\, dk \tag{105}$$

Figure 8: Vertical velocity (ms^{-1}) at $t = 40000\,s$ for the Schär test using semi-Lagrangian advection. The time step is $\Delta t = 8$, horizontal resolution $\Delta x = 250\,m$ and vertical resolution $H_T\,\Delta Z = 150\,m$.

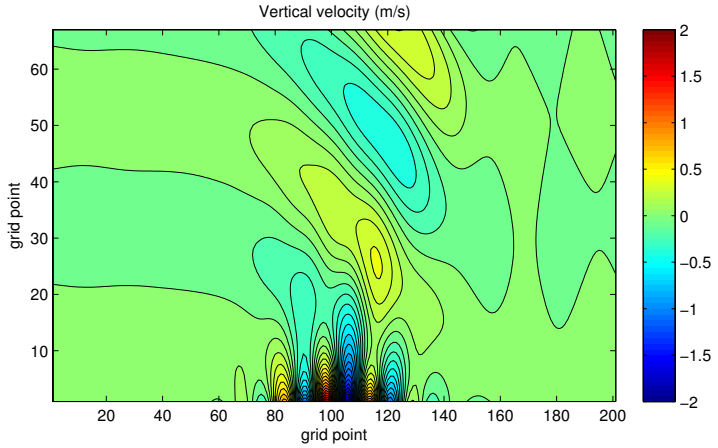

where $\hat{X} = X - U_0\,t$ and

$$\chi(k,\hat{X}) = \exp(-ak)\left(\cos\frac{k^2N^2\,t}{k^2+\pi^2/H_T^2} - 1\right)\cos k\hat{X} \tag{106}$$

The parameters for the test are the same as the non hydrostatic test reported in (Skamarock and Klemp, 1994). The Brunt-Väisälä frequency is $N = 0.01\,s^{-1}$, the upper boundary is placed at $H_T = 10\,km$, the perturbation half width is $a = 5\,km$ and the initial horizontal velocity is $U = 20\,ms^{-1}$. The horizontal and vertical resolutions are $500\,m$ and $250\,m$ respectively and the time step is $\Delta t = 6\,s$. The analytical and numerical solutions at time $3000\,s$ are shown in figures (9). The difference is due in part to the fact that the analytical linear solution and the non linear model do not have the same assumptions, the first being linear, Boussinesq and incompressible. In the numerical solution there is a vertical movement of the waves that is not present in the analytical solution. However horizontal wavelenght, phase speed and amplitude of both solutions are very similar.

It is considered here a non linear test with diffusion, consisting in a cold bubble in a neutral atmosphere, initially of elliptic shape at rest. For comparison, we follow the same test configuration as in (Straka, 1993) and (Janjic et al. 2001). Let us suppose a neutral atmosphere with a potential temperature of $\theta_0 = 300\,K$, and the following initial disturbance

Figure 9: Non hydrostatic inertial-gravity wave test, numerical and analytical solutions for the potential temperature at time $3000\ s$.

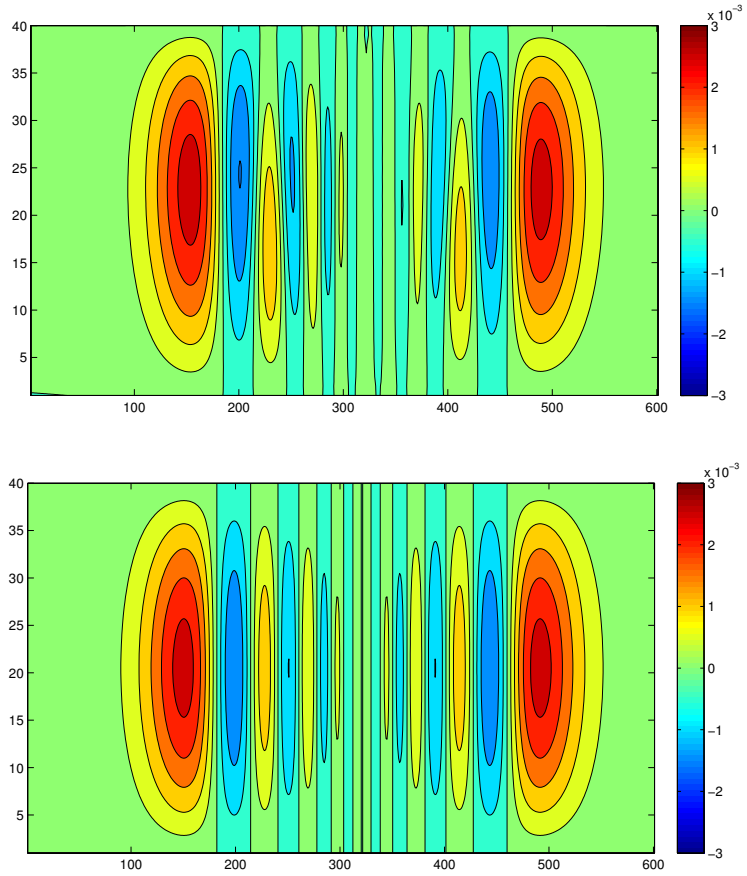

in the temperature

$$T'(x,z) = \delta T \, \cos^2\left(\frac{\pi d}{2}\right) \tag{107}$$

for

$$d \equiv \sqrt{\left(\frac{x-x_c}{x_r}\right)^2 + \left(\frac{z-z_c}{z_r}\right)^2} \leqslant 1 \tag{108}$$

where $\delta T = -15.0\,K$, $x_c = 0\,m$, $x_r = 4000\,m$, $z_c = 3000\,m$ and $z_r = 2000\,m$. The integration domain spans $25.6\,km$ in the horizontal direction and $6.5\,km$ in the vertical. The center of the initial disturbance is in the middle of the domain in the horizontal direction, which is the left boundary in the figures. The horizontal and vertical resolutions are $50\,m$. The time step is $0.15\,s$. Cyclic boundary conditions in the horizontal direction are used. The diffusion coefficient is $75\,m^2 s^{-1}$ for both components of the velocity and the temperature. Boundary conditions are: vertical velocity is zero at the boundaries and first derivative respect to vertical coordinate of temperature, pressure and horizontal velocity is zero at the boundaries.

The results of the test are good, when compared with the results of same test shown in figures 1 and 2 of (Janjic et al., 2001) and also figures 1 and 2 of (Straka, 1993). In figure (10) the potential temperature at times 0, 300, 600 and $900\,s$ is plotted.

9 Conclusions

A new dynamical kernel using a height based hybrid vertical coordinate and vertical finite elements discretization has been developed. The model is horizontally spectral and semi-implicit, being this aspects similar to the ALADIN non hydrostatic kernel. The Euler equations are used in coordinate-independent form. In particular, a covariant semi-Lagrangian scheme has been proposed and tested. The linear stability analysis shows that the model has a wide range of stability, although the height based vertical coordinate used is potentially less stable than the mass based vertical coordinate. A number of test taken from the literature has

Figure 10: Potential temperature, at times $0, 300, 600$ and $900\ s$.

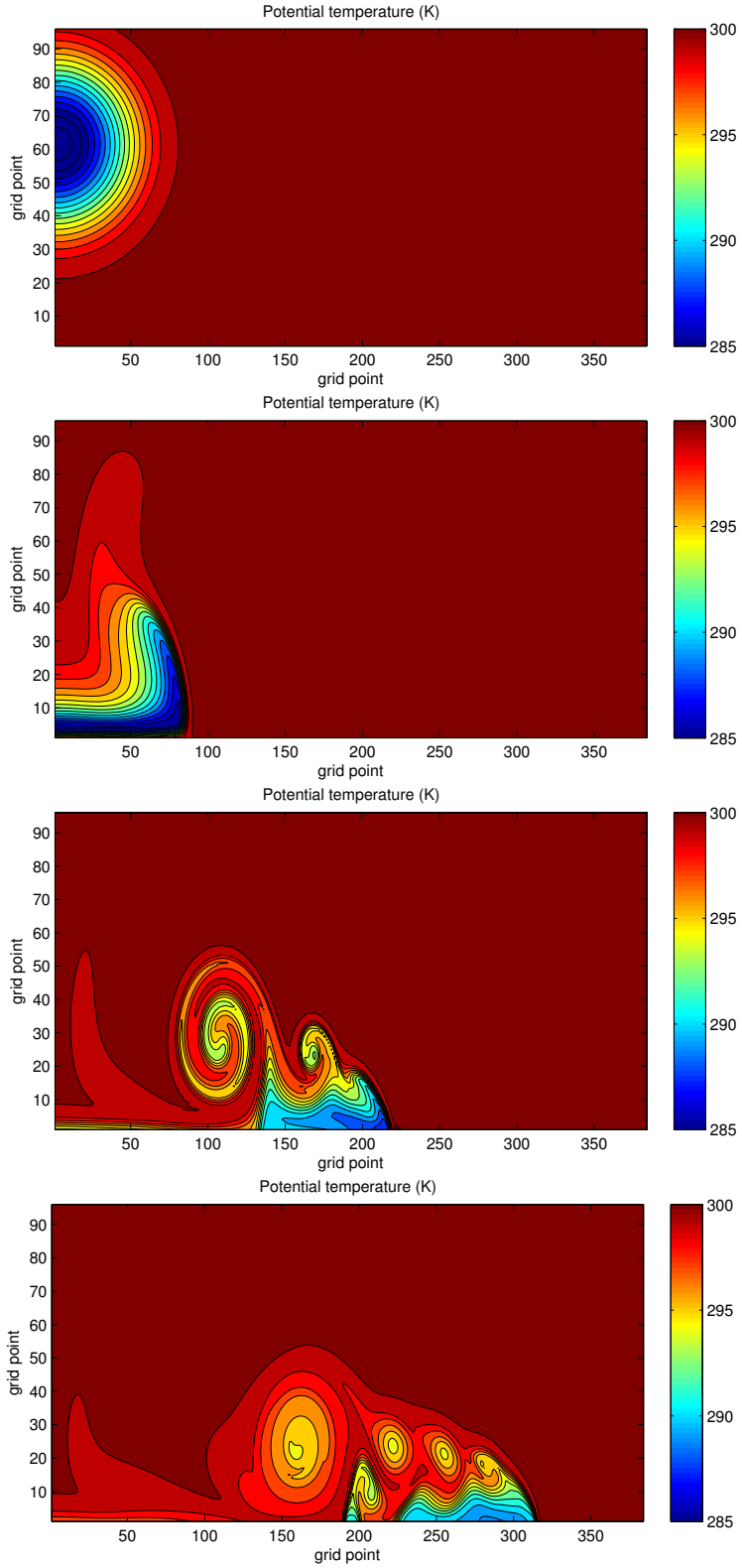

been used to verify the accuracy of the model.

References

[1] Arakawa A., Konor C. S. 1996. Vertical Differencing of the Primitive Equations Based on the Charney-Phillips Grid in Hybrid σ-p Vertical Coordinates. *Mon. Wea. Rev.* **124**: 511-528.

[2] Asselin R. 1972. Frequency Filter for Time Integrations. *Mon. Wea. Rev.* **100**: 487-490.

[3] Bär C. 2010. Elementary Differential Geometry. Cambridge University Press, 2010

[4] Bénard P. 2003. Stability of Semi-Implicit and Iterative Centered-Implicit Time Discretizations for Various Equation Systems Used in NWP. Monthly Weather Review *Mon. Wea. Rev.* **131**: 2479-2491.

[5] Bénard P., Laprise R., Vivoda J., Smolíková P. 2004. Stability of Leapfrog Constant-Coefficients Semi-Implicit Schemes for the Fully Elastic System of Euler Equations: Flat-Terrain Case. *Mon. Wea. Rev.* **132**: 1306-1318.

[6] Bénard P., Mašek J., and Smolíková P. 2005. Stability of Leapfrog Constant-Coefficients Semi-Implicit Schemes for the Fully Elastic System of Euler Equations: Case with Orography. *Mon. Wea. Rev.* **133**: 1065-1075.

[7] Bénard P., Vivoda J., Mašek J., Yessad K., Smith C., Brožková R. and Geleyn J. F. 2010. Dynamical kernel of the Aladin-NH spectral limited-area model: Revised formulation and sensitivity experiments. *Q. J. R. Meteorol. Soc.* **136**: 155-169.

[8] de Boor. 2001. A practical guide to splines, revised edition. Applied mathematical sciences 27. Springer-Verlag.

[9] Bubnová R., Hello G., Bénard P., Geleyn J. F. 1995. Integration of the Fully Elastic Equations Cast in the Hydrostatic Pressure Terrain-Following Coordinate in the Framework of the ARPEGE/Aladin NWP System. *Mon. Wea. Rev.* **123**: 515-535.

[10] Caya D., Laprise R. 1999. A Semi-Implicit Semi-Lagrangian Regional Climate Model: The Canadian RCM. *Mon. Wea. Rev.* **127**: 341-362.

[11] Côté J., Beland M. and Staniforth A. 1983. Stability of vertical discretization schemes for semi-implicit primitive equation models: Theory and application. *Mon. Wea. Rev.* **111**: 11891207.

[12] Cullen, M. J. P. 1993. The unified forecast/climate model. *Meteorol. Mag.* **122**: 81-94.

[13] Doms G., Schttler U. 1997. The Nonhydrostatic Area Model LM (Lokal-Modell) of DWD. Part I: Scientific Documentation. Deutscher Wetterdienst (DWD), Offenbach. March 1997.

[14] Dudhia J. 1993. A nonhydrostatic Penn State-NCAR Mesoscale Model: Validation tests and simulation of an Atlantic cyclone and cold front. *Mon. Wea. Rev.* **121**: 1493-1523.

[15] Gal-Chen T., Sommerville R. C. 1975. On the use of a coordinate transformation for the solution of NavierStokes. *J. Comput. Phys.* **17**: 209-228.

[16] Janjic Z. I., Gerrity Jr. J. P., Nickovic S. 2001. An Alternative Approach to Nonhydrostatic Modeling. *Mon. Wea. Rev.* **129**: 1164-1178.

[17] Kasahara A. 1974. Various vertical coordinate systems used for numerical weather prediction. *Mon. Wea. Rev.* **102**: 507-522.

[18] Klemp J., Skamarock W., Fuhrer O. 2003. Numerical Consistency of Metric Terms in Terrain-Following Coordinates. *Mon. Wea. Rev.* **131**: 1229-1239.

[19] Laprise R. 1992. The Euler Equations of Motion with Hydrostatic Pressure as an Independent Variable. *Mon. Wea. Rev.* **120**: 197-207.

[20] Luo H., Bewley T. R. 2004. On the contravariant form of the Navier-Stokes equations in time-dependent curvilinear coordinate sytems. *J. Comp. Phys.* **199**: 355-375.

[21] Ritchie H., Temperton C., Simmons A., Hortal M., Davies T., Dent D., Hamrud M. 1995. Implementation of the Semi-Lagrangian Method in a High-Resolution Version of the ECMWF Forecast Model *Mon. Wea. Rev.* **123**: 489-514

[22] Robert A. 1981. A stable numerical integration scheme for the primitive meteorological equations. *Atmos.-Ocean* **19**: 35-46.

[23] Robert A. 1982. A semi-Lagrangian and semi-implicit numerical integration scheme for the primitive meteorological equations. *J. Meteorol. Soc. Japan* **60**: 319325.

[24] Schär C., Leuenberger D., Fuhrer O., Lüthi D., Girard C. 2002. A New Terrain-Following Vertical Coordinate Formulation for Atmospheric Prediction Models *Mon. Wea. Rev.* **130**: 2459-2480

[25] Seifert A., Baldauf M., Stephan K., Blahak U., and Beheng K. 2008. The challenge of convective-scale quantitative precipitation forecasting. *15 th Int. Conf. Cloud and Precip.*, Cancun, Mexico, Preprints.

[26] Skamarock W., Klemp J. 1994. Efficiency and Accuracy of the Klemp Wilhelmson Time-Splitting Technique *Mon. Wea. Rev.* **122**: 2623-2630

[27] Straka J.M., Wilhelmson R.B., Anderson J.R., Droegemeier K.K. 1993. Numerical solutions of a non-linear density current: a benchmark solution and comparisons. International *Journal for Numerical Methods in Fluids* **15**: 1-22.

[28] Tanguay M., Robert A., Laprise R. 1990. A Semi-implicit Send-Lagrangian Fully Compressible Regional Forecast Model *Mon. Wea. Rev.* **118**: 1970-1980.

[29] Untch A., Hortal M. 2004 A finite-element scheme for the vertical discretization of the semi-Lagrangian version of the ECMWF forecast model *Q. J. R. Meteorol. Soc.* **130**: 15051530